

Wearable-informed generative digital avatars predict task-conditioned post-stroke locomotion

Authors

Yanning Dai^{1,2}, Chenyu Tang³, Ruizhi Zhang¹, Wenyu Yang¹, Yilan Zhang^{2,4}, Yuhui Wang², Junliang Chen¹, Xuhang Chen⁵, Ruimou Xie⁶, Yangyue Cao⁷, Qiaoying Li⁸, Jin Cao⁹, Tao Li¹⁰, Hubin Zhao¹¹, Yu Pan⁶, Arokia Nathan¹², Xin Gao^{2,4}, Peter Smielewski⁵, Shuo Gao¹

Affiliations

1 School of Instrumentation and Optoelectronic Engineering, Beihang University, 100191, Beijing, China

2 Centers of Excellence for Generative AI, King Abdullah University of Science and Technology, 23955, Thuwal, Saudi Arabia

3 Department of Engineering, University of Cambridge, CB2 1PZ, Cambridge, UK

4 Center of Excellence on Smart Health (KCSH), King Abdullah University of Science and Technology, 23955, Thuwal, Saudi Arabia

5 Brain Physics Laboratory, Division of Neurosurgery, Department of Clinical Neurosciences, University of Cambridge, Cambridge, CB2 0QQ, UK

6 Department of Physical Medicine and Rehabilitation, Beijing Tsinghua Changung Hospital, Tsinghua University, 100084, Beijing, China

7 Department of Rehabilitation, Beijing Tongren Hospital, Capital Medical University, 100005, Beijing, China

8 Stomatology and Rehabilitation Department, Shijiazhuang People's Hospital, 050000, Shijiazhuang, China

9 School of Life Sciences, Beijing University of Chinese Medicine, 100029, Beijing, China

10 Department of AI Medicine, The Fifth Medical Center of Chinese PLA General Hospital (301 Hospital), 100853, Beijing, China

11 Division of Surgery and Interventional Science, University College London, WC1E 6BT, London, UK

12 Darwin College, University of Cambridge, CB3 9EU, Cambridge, UK

Corresponding to: Chenyu Tang (ct631@cam.ac.uk) and Shuo Gao (shuo_gao@buaa.edu.cn)

Abstract

Dynamic prediction of locomotor capacity after stroke could enable more individualized rehabilitation, yet current assessments largely provide static impairment scores and do not indicate whether patients can perform specific tasks such as slope walking or stair climbing. Here, we present a wearable-informed data-physics hybrid generative framework that reconstructs a stroke survivor's locomotor control from wearable inertial sensing and predicts task-conditioned post-stroke locomotion in new environments. From a single 20 m level-ground walking trial recorded by five IMUs, the framework personalizes a physics-based digital avatar using a healthy-motion prior and hybrid imitation learning, generating dynamically feasible, patient-specific movements for inclined walking and stair negotiation. Across 11 stroke inpatients, predicted postures reached 82.2% similarity for slopes and 69.9% for stairs, substantially exceeding a physics-only baseline. In a multicentre pilot randomized study ($n = 21$; 28 days), access to scenario-specific locomotion predictions to support task selection and difficulty titration was associated with larger gains in Fugl-Meyer lower-extremity scores than standard care (mean change 6.0 vs 3.7 points; $p < 0.05$). These results suggest that wearable-informed generative digital avatars may augment individualized gait rehabilitation planning and provide a pathway toward dynamically personalized post-stroke motor recovery strategies.

I Main

Stroke is a leading cause of long-term motor disability and frequently results in persistent gait impairments such as hemiplegia, reduced joint mobility, and asymmetric movement patterns [1-3]. These motor deficits substantially limit independence, increase fall risk, and contribute to long-term healthcare burden. Globally, approximately 11.9 million people experience a stroke each year, and more than one-third of survivors retain chronic motor dysfunction despite months of rehabilitation [4, 5]. In many developing regions, disability rates can rise to 60–80 percent, reflecting not only the severity of post-stroke impairments but also the difficulty of delivering timely, intensive, and personalized rehabilitation [6-7].

Motor rehabilitation remains the most effective pathway for restoring function [3, 8-10], but its impact depends on how well task selection and dosing are matched to an individual patient's changing capacity. Clinicians continuously adjust cadence, incline, step height, and repetition to elicit targeted neuromuscular engagement while avoiding excessive fatigue, frustration, or injury risk [11-13]. To allow fine-grained quantification of gait and impairment in both laboratory and routine settings, advanced wearable sensing technologies have been introduced [14, 15]. Yet most existing pipelines compress rich time-series signals into static, descriptive outputs such as standardized clinical rating scales [16-18], kinematic movement-quality indicators [15, 19-21], and predicted recovery curves or performance scores [22, 23]. These summaries describe how a patient walked under an observed condition, but they fail to translate motion data into a dynamic, task-conditioned forecast of how the same individual is likely to move in a new rehabilitation scenario, which compensatory strategies will emerge, and where stability and safety limits are likely to be reached. Consequently, even when extensive wearables-generated assessments are available, therapists still rely on cautious trial-and-error when deciding, for example, whether a patient can safely progress to slope walking or stair training, which can lead to mismatched difficulty, suboptimal dosing, and delayed use of the critical rehabilitation window. The missing

capability is not a new way to measure gait, but a way to convert a brief, wearable-captured gait sequence into task-level, patient-specific predictions.

To address this gap, we introduce a wearable-informed generative framework that reconstructs each patient's locomotor control from a single 20 m level-ground walking trial recorded with body-worn inertial sensors, and uses the resulting control signature to predict task-conditioned post-stroke locomotion in new scenarios. The framework instantiates a patient-specific digital avatar by coupling a proportional-derivative physics controller with a Healthy Motion Atlas that captures normative gait coordination, and a goal-conditioned deep reinforcement learning policy that synthesizes individualized, dynamically feasible movements for two common yet challenging tasks: slope ascent and stair climbing. In this formulation, a brief wearable recording provides a minimal, scalable input from which the avatar can generate locomotion beyond the observed baseline while preserving patient-specific characteristics.

The avatar predicts task-specific locomotion after observing only the baseline walk: patient data drive personalization, whereas task training is obtained through large-scale exploration in the physics simulator, removing the need for task-specific demonstrations from patients. In a multi-centre study of 21 post-stroke inpatients across five rehabilitation centres, the model generated stable task-conditioned predictions for both slope and stair scenarios and reproduced individualized locomotion patterns, with predicted motions showing high similarity to measured task kinematics. To explore potential clinical utility, the cohort was further randomized into a model-assisted group ($n = 11$) and a control group ($n = 10$) for a 28-day pilot study; therapists in the model-assisted arm used the avatar's task-conditioned predictions to inform task selection and difficulty titration. Weekly Fugl-Meyer Assessment lower-extremity scores increased from 25.6 to 31.6 in the model-assisted group and from 26.0 to 29.7 in controls ($p < 0.05$). Together, these results suggest that task-conditioned locomotion predictions derived from a brief wearable recording may support individualized rehabilitation planning and reduce reliance on trial-and-error.

Together, the results establish the proposed generative model to transform wearable gait measurements into support for scenario-specific rehabilitation decisions. By transforming a short walking clip into actionable forecasts of task performance, compensatory strategy, and safety limits, the framework provides a mechanism to use wearable data for individualized planning rather than static description. The same principles hold the potential to be extended to more complex rehabilitation settings, broader neuromuscular conditions, and adaptive robotic assistance, moving toward continuously personalized and intelligent rehabilitation. Table S1 provides a comparative overview between the proposed generative model and state-of-the-art AI-assisted wearable approaches for rehabilitation.

II. Results

Overview of the Generative Rehabilitation Modelling Framework

We present a generative modelling framework that reconstructs each patient's control policy from a single 20 m walking clip and uses these personalized control signatures to generate task-conditioned locomotion for rehabilitation. This workflow begins with lightweight locomotion capture from healthy individuals and stroke patients (Figure 1a). A physics-driven digital avatar is then constructed, first by learning a population-level Healthy Motion Atlas and subsequently adapting it to each patient through goal-conditioned transfer (Figure 1b). The personalized controller generates task-conditioned locomotion across new rehabilitation scenarios (Figure 1c),

producing visualizations and activation patterns that reveal patient-specific abnormal or compensatory movement tendencies. These task-conditioned predictions inform clinician-guided planning by indicating which task levels can be safely attempted and which may induce compensations or instability (Figure 1d), ultimately supporting real-world rehabilitation decisions by guiding task and difficulty selection (Figure 1e). An end-to-end overview of the framework, with illustrative visualizations of key results, is provided in Supplementary Video 1.

In this study, a total of 21 post-stroke inpatients were recruited across five rehabilitation centers (Beijing Tsinghua Changgung Hospital, Beijing Tongren Hospital, Shijiazhuang People's Hospital, Beijing University of Chinese Medicine, and the Fifth Medical Center of the Chinese PLA General Hospital). Patients were randomly allocated to a model-assisted group ($n = 11$) or a control group ($n = 10$). Unless otherwise stated, all personalized modelling and quantitative evaluations reported below refer to the model-assisted group.

Data Acquisition and Physics-based Avatar Establishment

We construct a unified gait locomotion dataset and develop a physics-based digital human model to support subsequent analyses. Motion data is captured using five inertial measurement units (IMUs) mounted on the pelvis, thighs, and shanks (Figure 2a), with signals transformed from the Earth Coordinate System (ECS) into the Joint Coordinate System (JCS) to obtain anatomically consistent joint representations [24]. Detailed participant recruitment and data-collection procedures are provided in the Methods section.

A lower-limb digital avatar is implemented in Unity 3D with PhysX physics simulation engine (Figure 2b), featuring a six-degree-of-freedom pelvic root and nine actuated lower-limb degrees of freedom controlled via proportional-derivative (PD) torque actuation. Contact constraints, joint coupling, and non-slip conditions were enforced to suppress sensor-induced artifacts such as floating, vibration, and ground penetration. Model parameters and joint specifications are summarized in Table S2 and follow established anatomically consistent musculoskeletal models [25, 26]. The recorded sequences were processed through a unified pipeline (Figure 2c-d): denoised joint trajectories were segmented into single-step clips using each subject's dominant gait frequency, then further refined via the physics-based model to eliminate sensor-induced artifacts.

The resulting dataset includes 162 healthy-walking clips and 21 post-stroke clips, totalling 21,674 frames. The joint distribution of step length and walking speed (Figure 2e) shows that healthy locomotion spans the range exhibited by post-stroke subjects, enabling healthy-calibrated models to adapt to patient-specific gait patterns. Representative trajectories (Figure 2f) highlight impaired-gait characteristics—including reduced step length, asymmetric stance phases, and compensatory circumduction [27, 28]. Additional visualizations are provided in Figure S1.

Healthy Motion Atlas Performance Evaluation

The control framework integrates reinforcement learning with a physics-based human model to establish a population prior of normative gait, termed the Healthy Motion Atlas (HMA). As shown in Figure 3a, the controller is a policy network $\pi(a|s)$ optimized using Proximal Policy Optimization (PPO) [29]. The network receives a compact state vector s_t containing the motion phase, target variables (walking speed and step length goals), PD control parameters, body posture and velocity features, and environmental interaction cues. It outputs activation signals a_t that serve as target joint angles and torque bounds for the PD controller. Figure 3b details the composition

of the state input. The full simulation–learning pipeline (Figure 3c) couples Unity and PhysX physics for dynamic simulation, PyTorch for neural policy learning, synchronized via a real-time parameter interface. Figure 3d outlines the PPO update structure, where trajectory collection and policy optimization form a repeated loop that progressively refines the controller.

The HMA is trained to capture population-level gait dynamics from healthy-walking clips, encoding coordinated patterns of state – activation evolution. Over 230 million environment steps (≈ 4 days 8 h), the controller progresses through three characteristic phases: initial standing (0–1 M), transient forward falling (≈ 1 –3 M), and stable stepping emerging beyond 3 M steps. Convergence occurs around 180 M steps, producing a stable, cycle-consistent policy that maintains rhythmic locomotion and serves as a foundation for individualized patient adaptation. The training curves for cumulative reward and sequence length are shown in Figure 3e.

To evaluate generalization, we examine performance across combinations of target speed and step length. The distribution of normalized rewards remains broadly uniform within the trained range, with the highest accuracy at moderate speeds (0.5–1.1 m/s) and step lengths (1.2–1.8 m)—patterns consistent with human walking. Sensitivity analyses and control-accuracy maps are presented in Figure 3f and Figure S2, while joint- and endpoint-level errors are summarized in Figure S3, indicating a mean single-axis joint-angle error of 11.61° , Center-of-Mass (CoM) error of 2.69 cm, and end-effector error of 12.32 cm. These results demonstrate that the Healthy Motion Atlas achieves stable, biomechanically coherent gait control suitable for downstream clinical adaptation.

Atlas-to-Patient Clinical Adaptation Performance Evaluation

The Atlas-to-Patient Clinical Adaptation module fine-tunes the HMA to patient-specific gait characteristics through transfer learning. Atlas-to-patient adaptation and all subsequent personalized evaluations were conducted on the model-assisted patients group ($n = 11$). As shown in Figure 4a, the personalized controller inherits the pretrained state–activation policy from the Atlas and is fine-tuned on each patient’s data. This adaptation leverages population-level coordination patterns while allowing the controller to adjust its parameter set to capture individual impairments and control dynamics.

Figure 4b illustrates representative adaptation dynamics and control performance for a single patient, tracking the evolution of multiple reward components, including root position and velocity, the step-length and posture imitation terms, as well as the cumulative reward and overall episode length. Each sub-reward shows gradual stabilization, confirming that the personalized controller progressively aligns with the target walking pattern. Using the trained patient-adapted policy, 500 repeated evaluation trials were conducted under prescribed goals of 1.02 m/s walking speed and 0.80 m step length. The resulting outcomes (Figure 4c) show mean values of 0.98 m/s and 0.7626 m, with bars representing means and error bars denoting the 25th/75th percentiles. These results indicate accurate tracking of both temporal and spatial gait parameters within the patient’s natural rhythm.

Figure 4d provides a group-level summary across the 11 patients, reporting individual joint- and position-level control accuracy aggregated over repeated walking trials. Mean single-axis joint-angle errors are 5.48° across lower-body articulations, together with 1.67 cm CoM deviation and a 6.35 cm end-effector error. Compared with the healthy atlas controller, these errors are reduced to 47.2%, 42.4%, and 51.5% of baseline values, respectively, confirming both efficiency and stability of individualized learning. Full learning-curve, performance, and efficiency comparisons between atlas-initialized and scratch training are provided in Table S3 and Figure S4,

demonstrating that atlas initialization substantially accelerates convergence while maintaining biomechanical coherence.

Terrain-Adaptive Locomotion Prediction

The locomotion-prediction framework integrates behaviour cloning (BC) and a generative adversarial imitation learning (GAIL) [30] objective to guide the optimisation of the physical controller (Figure 5a). BC provides early stabilisation of state–activation alignment, whereas GAIL provides an intrinsic imitation-based reward that encourages the controller to preserve the consistency of activation signals throughout the motion sequence, ensuring that the generated control commands maintain both physiological plausibility and patient-specific rhythm. We evaluate the framework on clinically representative rehabilitation tasks of increasing difficulty—slope ascent and stair climbing—trained under a curriculum that progressively increases task demands. Illustrative results are presented for a representative ambulatory stroke case exhibiting left-sided impairment yet preserved independent mobility, with nominal level-ground parameters of 0.707 m/s walking speed and 0.801 m step length.

Task I - Slope Ascent

Training on the slope-ascent task required approximately 23 million environment steps (≈ 8 h). Across 5 curriculum levels, both task difficulty and associated reward components (Figure 5b and Figure S5a) showed clear progression and stable convergence. Throughout learning, the controller consistently preserved the patient’s characteristic gait features—limited knee flexion, circumduction during swing, and compensatory pelvic hike—despite the increasing terrain demands. The step budgets needed to complete successive curriculum levels rose with difficulty (0.7 M, 2.3 M, 4.7 M, 5.9 M, and 9.4 M), reflecting the added control complexity.

GAIL-related metrics, including internal imitation reward, discriminator output, and discriminator loss, further indicate stable optimisation (Figure S6). The discriminator output remained close to 0.5 throughout training, demonstrating that the generated activation patterns closely matched the patient’s flat-ground motion activation signals and that the controller preserved the patient’s motion activation style under new slope conditions. To quantify this alignment, we introduce an activation-signal imitation metric, which measures pattern-level similarity between generated and patient activation sequences; under slope conditions, this metric reached 99.70% (details presented in Table S4).

Task II - Stair Climbing

For stair climbing, we adapt a five-level curriculum with progressively increasing step height. Under curriculum progression, the cumulative reward and episode length grow smoothly and then plateau, indicating stable mastery (Figure 5b). Step budgets also increase with difficulty (11.3 M, 13.4 M, 26.1 M, 43.9 M, and 57.3 M). Detailed training curves of all reward components are provided in Figure S5b. To address the known difficulty of producing natural stair gaits in example-guided DRL [31], we introduce a minimal terrain-aware guidance reward that encourages a leg-raising action when a step is detected ahead; we also report a +guidance/-guidance ablation. Without this cue, the policy fails to mount the stairs and oscillates near the edge, underscoring the need for task-aware shaping. The definition of this guidance term and additional analyses are provided in Methods. Figure 5c shows the intrinsic reward and discriminator output during GAIL-based stair adaptation. Using the same activation-signal imitation metric, the stair-task consistency reaches 79.72% (Table S5).

The data-physics hybrid controller shows strong robustness. Perturbation tests [31, 32] (Table S6) indicate that it withstands forward disturbances up to 980 N and lateral disturbances up to 320–360 N while maintaining balance. A baseline comparison (Figure S7; Table S7) further demonstrates that the data–physics hybrid converges on a 1:12 slope in \approx 23 M steps versus \approx 90 M for a physics-only controller (DeepMimic [31])—requiring only 25.56% of the original training time—while delivering +4.73% higher joint-angle imitation accuracy and +12.10% distal-endpoint accuracy.

Figure 5d reports average patient-specific task posture prediction accuracy across the model-assisted group ($n = 11$), by comparing generated motions with measured kinematics in real-world tasks. Accuracy is quantified using the same posture similarity metric as the imitation reward (Supplementary Note S1). Two reference levels are shown to contextualize the prediction accuracy. First, an 87% simulation reconstruction accuracy is shown as an upper reference, obtained by reconstructing recorded patient motion in physics-based simulation. It reflects unavoidable wearable-sensor noise, drift, and minor variations in sensor placement and body dimensions, together setting a practical accuracy limit for posture comparison. Second, a flat-to-task gait deviation reference is shown, computed using the same posture similarity metric, to quantify the natural gait change when transitioning from flat-ground walking to slope or stair locomotion (averaging \sim 75% for slopes and \sim 48% for stairs). Across the 11 patients, the results show 82.2% posture similarity on slopes and 69.9% on stairs, demonstrating accurate prediction of task-specific gait patterns, with performance well beyond the natural deviation from flat-ground walking and close to the simulation reconstruction limit. Figure 5e then shows representative visualized rollouts across difficulty levels (pass vs. unsafe) for slopes and stairs, illustrating how the system visualizes success and flags risk; for example, low stair height (7.5 cm) yields stable ascent, whereas high stair height (15 cm) induces excessive lateral trunk sway (56.1°), signalling a safety boundary for the current stage. These results endorse the proposed generative framework as an effective and reliable paradigm for patient-specific locomotion prediction.

Clinical Integration and Rehabilitation Outcomes

To evaluate clinical usability, the proposed data – physics hybrid generative model is deployed across the five rehabilitation institutions (Figure 6a). At each site, the workflow followed a unified clinician-in-the-loop protocol. Upon admission, every patient completed a 20 m level-ground walking test, which served as the sole input for constructing the individualized model. Using this single clip, the system generated patient-specific simulations for slope ascent and stair climbing tasks. Therapists at each hospital reviewed the predicted gait trajectories and the associated activation-signal visualizations to examine whether the patient could maintain stability, where compensatory movements might emerge, and how task difficulty should be adjusted. The system did not prescribe exercises; instead, it served strictly as a decision-support tool, allowing clinicians to incorporate model-generated insights into their own professional judgement. This ensured that therapist expertise—patient fatigue, comorbidities, motivation, and safety considerations—remained central to individualized treatment planning across all five sites. Therapist-reported feedback further indicated that the system integrated well into routine clinical workflows, imposed acceptable time burden, and provided clinically interpretable and actionable information for rehabilitation planning (Figure 6c).

A pilot clinical study was then conducted using this deployment. The same 21 post-stroke patients with lower-limb motor impairment (model-assisted, $n = 11$; control, $n = 10$) received standard

lower-limb rehabilitation for 28 days, with weekly FMA-lower-extremity (FMA-LE) assessments [33] performed by blinded therapists (Figure 6b). At baseline, impairment levels were comparable between groups (control: 26.0; model-assisted: 25.6). Over the four-week period, however, patients whose therapists used the proposed generative model's predictions exhibited faster functional improvement. By day 28, the model-assisted group achieved an average FMA-LE score of 31.6, whereas the control group reached 29.7, a statistically significant difference ($p < 0.05$). Consistent with these findings, patients reported high acceptability of the wearable-based 20 m walking assessment, with favorable ratings for comfort, safety, and willingness to repeat the procedure during rehabilitation (Figure S8).

These results demonstrate that the proposed dynamic, task-predictive generative model provides clinicians with actionable, scenario-specific insights that conventional static assessment methods cannot offer. By enabling therapists to preview patient-specific performance in slope and stair tasks, the system supports more accurate task selection, safer difficulty modulation, and better alignment between training intensity and individual capability. This clinician-in-the-loop decision support ultimately contributes to more efficient and effective recovery trajectories in lower-limb post-stroke rehabilitation.

III. Discussions

This study advances a new paradigm for wearable-based motor rehabilitation by shifting wearable data processing from static, descriptive assessment to dynamic, visualised task performance prediction. Rather than treating wearable gait signals as endpoints for static scoring or descriptive analytics, we demonstrate how a brief, wearable-captured walking sequence can be transformed into a patient-specific, generative representation of locomotor capacity across unobserved rehabilitation tasks. By integrating wearable-derived kinematics with a physics-based control model, a population-level Healthy Motion Atlas, and goal-conditioned reinforcement learning, the proposed framework reconstructs individualized locomotor control signatures and uses them to generate dynamic predictions for clinically meaningful mobility challenges such as slope ascent and stair climbing. In doing so, wearable data are elevated from passive measurements that underpin static, metric-based predictions to active drivers of dynamic, task-conditioned decision support grounded in physically plausible motion. The resulting simulations preserve patient-specific movement style, achieve high fidelity at joint and endpoint levels, and remain physically consistent, while requiring only minimal wearable input. Together with multi-center pilot results showing significantly improved Fugl–Meyer lower-extremity outcomes when these predictions are used in planning, this work establishes a practical and scalable wearable-centered framework for anticipating task feasibility, progression difficulty, and personalized intervention in post-stroke mobility rehabilitation.

Several considerations temper the interpretation of these findings. First, our evaluation focused exclusively on two rehabilitation scenarios, slope walking and stair climbing. These tasks are among the most common and clinically consequential in gait retraining [34, 35], yet they do not encompass the broader range of activities encountered in rehabilitation practice, such as turning, dual-task walking, robot-assisted gait training, or perturbation-based balance tasks [36]. Extending the model to these scenarios will require expanding the controller's action space and incorporating terrain- or device-specific dynamics. Second, our current patient cohort consists of stroke survivors who are able to walk independently without assistive devices. The present framework is therefore

tailored to this functional subgroup and does not directly generalize to individuals who rely on canes, walkers, or caregiver support. Extending the system to these populations will necessitate explicit modeling of assistive-device interactions, more complex human – device dynamics, and larger multi-center datasets to capture broader clinical variability. Third, as with any simulation-based prediction, performance in novel tasks cannot be directly verified at the moment of use. The system should therefore be understood as a decision-support tool rather than a replacement for clinical judgement, and its task recommendations should be interpreted in conjunction with therapist expertise and patient-specific constraints. Future prospective trials will be required to calibrate uncertainty, validate safety thresholds, and establish evidence-based standards for clinical adoption.

Despite these limitations, the proposed framework holds significant promise for the future of neurorehabilitation. By enabling low-cost, cross-clinic prediction of task-specific motor capability from minimal data, the method may improve personalized treatment planning for stroke and other neuromuscular or neurodegenerative disorders. Because the controller embeds musculoskeletal and neuromotor constraints within a physics-based environment, the underlying principles can, in concept, be adapted to conditions such as Parkinson's disease, cerebral palsy, and spinocerebellar ataxia with appropriate task and data adjustments. In this sense, the approach can be viewed as an early step toward a human body digital twin for lower-limb motor function, in which continuously updated, individualized simulations mirror a patient's evolving gait capacity and constraints [37]. Moreover, as the system is deployed in practice, its continuous use could be integrated with active-learning strategies to iteratively refine the underlying models, progressively building a richer, rehabilitation-centered representation of human motor behavior. Such a data-driven evolution could generate new insights into disease mechanisms, task difficulty progression, and recovery trajectories. In the longer term, once robustness and generalization are established, this modeling paradigm may support scalable, remotely delivered rehabilitation guidance in under-resourced or underserved regions, helping to democratize access to personalized, high-quality neurorehabilitation worldwide.

IV. Methods

Data Collection Protocol and Participant Recruitment

To support individualized controller learning and task-conditioned locomotion prediction, we constructed a lower-limb gait dataset from controlled clinical trials and a supplementary public motion-capture repository. Participants for the clinical component were recruited from Beijing Tsinghua Changgung Hospital, Beijing Tongren Hospital, Shijiazhuang People's Hospital, Beijing University of Chinese Medicine, and the Fifth Medical Center of the Chinese PLA General Hospital (301 Hospital) under approved institutional protocols and informed consent procedures. The patient cohort comprised 21 individuals with post-stroke hemiparesis in the mid-recovery phase (1–6 months post-stroke), all of whom were able to stand and walk independently. Demographic variables—including age, sex, height, weight, affected side, and time since stroke—are reported in Table S8. To provide reference locomotion patterns, an additional 19 healthy adults were recruited under the same protocol.

All clinical participants completed habitual-pace straight walking along a 20 m level walkway. Lower-limb kinematics were recorded using five Perception Neuron 3 nine-axis IMUs placed on the pelvis, bilateral thighs, and bilateral shanks (90 Hz sampling; 0.02° pose resolution) [38]. Sensor

placement was standardized across individuals to ensure consistent measurement of segment rotations and translations. To broaden dataset coverage and to enrich the representation of high-quality nominal gait cycles, we further incorporated 67 straight-walk sequences from the CMU Motion Capture database (optical capture at 120 Hz) [39]. Statistics for each cohort—including the number of clips, average duration, sampling rates, and cycle-to-cycle consistency—are summarized in Table S9. Following the acquisition, all recordings were denoised and segmented into single-step clips using the processing pipeline described in the Results Section. Clips with unstable intra-cycle structure were excluded to ensure that retained segments reflect reliable and representative gait behavior for each subject.

Control Policy Formulation

We define the avatar’s control policy $\pi(a_t | s_t)$ that outputs the motor activation a_t given the simulated state s_t at time t . The policy is optimized to generate motions that match the reference posture P_t at each time step. The human motor-control system is highly complex and underdetermined, making it impractical to derive a closed-form equation for the activation signal a_t . To address this, we employ DRL techniques to learn a control policy network [40] through iterative trial-and-error interaction with the environment, during which the policy updates its parameters based on feedback from each $s_t - a_t$ transition.

Our model builds upon the Deepmimic framework proposed by Peng et al. [31], a widely used framework in physics-driven motion generation tasks due to its robustness and high fidelity in mimicking reference actions. In this study, we expanded its inputs beyond fixed body postures to include arbitrary goals like walking speed, step length, and cadence, as depicted in Figure 3a. This extension enables the model to learn diverse walking patterns from healthy individuals, thereby accelerating the adaptation process and facilitating personalized control-policy training for patients.

States and Activation Signals

The input state signal s comprises five main components, as illustrated in Figure 3b: (i) phase [0, 1], which aligns the current frame to the target frame for sequence imitation and removes the need to feed target actions directly (improving compactness and scalability [41]); (ii) motion goal (target walking speed, step length, and their deviations from the current state); (iii) PD control information (per-joint torque upper limits); (iv) body posture: root height/rotation, each child node’s local rotations plus linear/angular velocities, as well as CoM and limb-endpoint positions relative to the root (all angles in quaternions); and (v) environment interaction: foot–ground contact (0/1), hip–ground distance, and terrain rays cast near the root over the past three frames. Rays span the sagittal plane from -90° to 90° , cast at 45° increments (13 rays total). This range-sensing approach is more efficient than height maps or image inputs while still supporting complex terrain (e.g., stairs) and improving stability. In total, the state vector comprises 122 motion state variables.

The activation signal a consists of two parts: target rotation angles for each joint in the PD controller, and the upper limits of joint torques. The dimensions of the target rotation angles align with the degrees of freedom (DoF) of the controllers, while the joint torque limits specify the maximum torque for each joint, totaling 14 dimensions.

Reward

During policy training, each action a_t produced by the controller is evaluated through a reward signal, which provides feedback on how desirable the action is for the task and guides the improvement of the policy over time. The reward function r_t follows prior work [31, 42], and is

formulated as a weighted sum of a goal-completion reward r_{goal} , a locomotion-imitation reward $r_{imitation}$, and a physical-feasibility penalty $p_{physics}$. However, instead of computing the goal reward r_{goal} independently at each frame as in prior work, we evaluate each goal parameter over a short temporal window. This aggregation over time reduces frame-to-frame fluctuations and mitigates cumulative drift in the controller. The reward function r_t is defined as:

$$r_t = w_1 r_{goal} + w_2 r_{imitation} - p_{physics}$$

where w_1 and w_2 are both set to 0.5. In this formulation, r_{goal} matches global gait targets (walking speed, step length, forward direction, and root pose stability), $r_{imitation}$ preserves local style and coordination (joint angles/velocities, CoM, and distal endpoints), and $p_{physics}$ penalizes non-physical contacts (e.g., foot sliding and mid-air floating) with early termination on non-foot ground contacts. Full mathematical definitions are provided in Supplementary Note S1.

Atlas-to-Patient Control Model: Policy Representation and Optimization

Policy Representation

The control policy π is represented by a feedforward neural network that maps a given state s to a motor-activation signal a . The signal a is modeled as a Gaussian distribution $a \sim N(\mu(s), \Sigma)$, where the mean $\mu(s)$ is produced by the network, and the covariance matrix Σ is assumed diagonal and parameterized as $\Sigma = \varphi I$, where I is the identity matrix and φ is a hyperparameter controlling action noise. The network contains three hidden layers with 256 units each, using ReLU activations throughout. The policy input is a 122-dimensional state vector; to enrich temporal observation, we stack three consecutive frames ($t-2, t-1, t$), yielding a 366-dimensional final input. The policy outputs a 14-dimensional motor activation signal vector.

During network training, a current state s_t is fed into the policy network π to obtain the activation signal a_t , which is then applied to the joint PD controllers for forward dynamics simulation, producing the next state s_{t+1} . The state s_{t+1} is compared with the reference data to compute the reward r_t at time t . The training objective is to learn a policy that maximizes the expected cumulative reward over each rollout. To optimize the policy π , we employ the Proximal Policy Optimization (PPO) algorithm [29], a widely used and robust method for continuous-control problems. This process involves training both the policy network and a separate value function network. The value network is trained in parallel to estimate state values; it is also a feedforward neural network with two hidden layers of 128 units each, using the same input state representation but producing a single scalar value estimate.

Training Procedure

Network training proceeds in two stages: Healthy Motion Atlas Construction (HMA) and Atlas-to-Patient Clinical Adaptation (A2P-CA). Simulation and policy execution run at 30 Hz. Each episode is capped at 500 time steps and terminates early upon reaching the cap or detecting a fall. PPO updates occur after collecting 204,800 samples, using a batch size of 2,048 and a reward discount factor of 0.995. All remaining settings (e.g., update cadence, learning-rate schedules) are listed in Table S10.

- Stage I — Healthy Motion Atlas Construction

We first construct a normative motion atlas from 162 healthy walking clips (21,674 total time steps). At the beginning of each episode, a target walking speed and step length are randomly sampled from training ranges (0.4–1.4 m/s for speed and 0.5–1.7 m for step length). A reference

clip is then selected from the healthy gait dataset as the one whose (speed, step length) pair is closest to the sampled target in Euclidean distance. The reference clip is then time-resampled so that its walking speed and total number of frames match the sampled target. This stage yields a healthy baseline model capable of generating gait patterns across a broad range of locomotion conditions.

- Stage II — Atlas-to-Patient Clinical Adaptation

The atlas policy is then adapted to each stroke patient via transfer learning, reducing time and computation while improving generalization, compared with training a patient-specific model from scratch. In this stage, the imitation reference is replaced with a patient-specific walking clip, so the policy learns to match the individual’s gait patterns rather than the healthy atlas. Accordingly, the target walking speed and step length in the state s_t are fixed to the patient’s observed values. This adaptation preserves the atlas-level motion structure while enabling the controller to capture patient-specific characteristics essential for personalized rehabilitation.

Personalized Locomotion Prediction Framework

Data-Physics Hybrid-Driven Model Architecture

Building on the individualized control policy, we propose a data-physics hybrid-driven motion generation framework for a range of rehabilitation tasks. Existing DRL-based motion frameworks often rely on hand-crafted rewards and heavy tuning, and manual interventions that may introduce bias. To mitigate these issues, we combine behavioural cloning (BC) [43] for warm starts with GAIL for continual consistency checks of the patterns between generated and real activation signals. Additional context on the broader motion-generation landscape relevant to this framework is provided in Supplementary Note S2.

For different rehabilitation tasks, we make only minor adjustments to the model’s states, activation signals, and rewards:

- *State s' :* Add or modify only task-specific goal information (e.g., distance-to-path for trajectory following, or adjusted target speed).
- *Activation signal a' :* Retain the same definition as in the individualized controller.
- *Reward r' :* Keep the original structure; only update the global targets in r_{goal} (such as speed, step length, direction) according to the requirements of each task. For challenging tasks, sparse auxiliary cues may be introduced during early training to aid convergence, with negligible effect on final behavior.

This design minimizes manual engineering, improves physiological interpretability, and enhances predictive flexibility in complex and unfamiliar scenarios.

Training Procedure

Locomotion prediction is learned from a single motion clip of each patient. For a given rehabilitation task g , the original state and activation sequences $\{s, a\}$ are transformed into their task-conditioned forms $\{s', a'\}$. For clarity of notation in this section, we denote the patient’s transformed reference data as $\{s'_{ref}, a'_{ref}\}$. During model training, simulated rollouts generated by the policy are written as $\{s'_{sim}, a'_{sim}\}$, and the learnable policy network is denoted by π' . The training procedure is divided into two phases: behavioral prior distillation and generative adversarial task prediction.

- Stage I — Behavioral Prior Distillation (BPD)

In BPD, a behavior-cloning proxy π_{BC} is trained in a supervised manner on the patient's reference clip, using s'_{ref} as inputs and a'_{ref} as outputs. The trained proxy is then duplicated to initialize the policy network π' , including architecture and parameters, thereby injecting a patient-specific behavioral prior before locomotion prediction. When the rehabilitation setting satisfies $s'=s$ (i.e., the policy's observation space already matches the reference), this phase can be skipped by directly setting $\pi'=\pi$.

- Stage II — Generative Adversarial Task Prediction (GATP)

GATP adapts the initialized policy π' to the rehabilitation task through a combination of behavioral imitation, GAIL-based adversarial learning, and physics-driven reinforcement learning. At each simulated state s'_{sim} , the policy π' outputs an activation a'_{sim} , while the fixed behavioral-cloning proxy π_{BC} produces its reference activation a'_{BC} . Their discrepancy defines a supervised imitation loss $L_{BC} = \|a'_{sim} - a'_{BC}\|$, which helps preserve patient-specific activation characteristics. This term is added to the standard PPO loss [29] with coefficient α_{BC} , which linearly decays from 0.2 to 0 over the first 5 M steps so that the contribution of BC supervision gradually diminishes as reinforcement learning progresses. In parallel, the GAIL discriminator D_θ compares a batch of generated pairs (s'_{sim}, a'_{sim}) with real patient pairs (s'_{ref}, a'_{ref}) sampled from the reference clip, learning to distinguish the two underlying distributions. Its output is converted into a per-timestep intrinsic imitation reward r_{in} , which is combined with the physics-based external reward during PPO updates:

$$r_{in}(s, a) = -\log \left[1 - D_\theta \left((s_{sim}, a_{sim}), (s_{ref}, a_{ref}) \right) \right]$$

Meanwhile, the physics-based controller provides an external reward $r_{ex} = r'$. PPO then optimizes π' using the combined reward $r_{tot} = r_{ex} + r_{in}$, producing an update step informed jointly by physical feasibility and imitation fidelity. The final parameter update further incorporates the behavioral-cloning supervision term weighted by α_{BC} , yielding a controller that retains patient-specific activation characteristics while adapting robustly to the rehabilitation task.

The policy and discriminator networks are feedforward networks (policy 3×256; value and discriminator 2×128, ReLU). We linearly decay PPO/GAIL learning rates ($2 \times 10^{-5}/1 \times 10^{-5}$) and weight external/internal rewards at 0.9/0.1.

Task-Conditioned Rehabilitation Evaluation

This study presents two training scenarios involving typical tasks for patients in daily life and rehabilitation training: slope ascent and stair climbing. Curriculum Learning (CL) techniques [44] are employed to adjust task difficulty, such as varying slope angles and step heights, and accelerate convergence by adapting learning speed. We apply CL to set five difficulty levels for each task. Difficulty is promoted when the cumulative reward exceeds 90% of the patient's flat-ground performance (280) and after at least 500 episodes.

Task I - Slope Ascent

We evaluate performance while maintaining the patient's nominal speed and step length across a five-level curriculum from flat ground to a final 1:12 incline. The ramp is 9 m long with elevations 0, 0.1875, 0.375, 0.5625, 0.75 m. Slope is computed as: slope = (height difference/vertical distance) × 100%. In real life, outdoor ramps for disabled individuals typically have slopes ranging from 1:12 to 1:20.

Task II - Stair Climbing

We train and evaluate the patient-specific controller to climb stairs without preset speed targets, following a five-level schedule with step heights of 0, 3.75, 7.5, 11.25, 15 cm (typical real-world steps: 10–15 cm height, 30 cm depth). This task tests the method on clinically challenging rehabilitation scenarios. Prior work shows that example-guided DRL often struggles in stair environments because of large mismatches between reference actions and task objectives [45,46]. To mitigate this, we introduce a minimal terrain cue: if a step is detected within 5 cm ahead of the foot, a leg-raise action receives reward 1 (otherwise 0; if no step is ahead, reward 1). The cue only facilitates initial learning and is disabled once mastery is achieved, preserving final motion predictions [45]. Task environments are visualized in Figure S9. Integrated metrics of curriculum mastery and movement quality translate into patient-specific task and difficulty recommendations, supporting safe and targeted rehabilitation planning.

Clinician Use of Simulated Rehabilitation Videos

For each enrolled patient, the generative model produced short, patient-specific simulation videos of slope ascent and stair climbing at predefined difficulty levels, using only the 20 m level-ground walking trial as input. Rehabilitation physicians or physical therapists view these videos alongside routine clinical information to judge whether a given task level was likely to be feasible, to anticipate potential compensatory movements, and to adjust the starting difficulty or progression speed of conventional lower-limb training. The system does not generate explicit prescriptions or "safe/unsafe" labels; it serves purely as a visual decision-support aid. All final decisions regarding task selection, intensity, and progression follow local clinical guidelines and the independent judgment of the treating clinician.

Computational Environment and Resources

All simulation scenes and 3D assets are built and rendered in Unity 3D; rigid-body dynamics are computed by NVIDIA PhysX. Reinforcement learning and control interfaced with the simulator via Unity ML-Agents (Release 20), with training implemented in PyTorch 1.8.0 (CUDA 11.1) on Python 3.8.13. Experiments run on a workstation equipped with an NVIDIA GeForce RTX 3090 (24 GB VRAM) and an Intel i7-12700 (12 cores, 2.10 GHz); the control/physics loop operated at 30 Hz. Detailed hyperparameters are provided in Table S10.

Data Availability

All data supporting the findings of this study are publicly available at: <https://github.com/YanningDai/StrokeAvatar.git>. The repository includes de-identified gait sequences from 19 healthy individuals and 21 stroke patients, as well as processed kinematic features used for model training and evaluation.

Code Availability

The full implementation of the proposed data–physics hybrid generative framework is publicly available at: <https://github.com/YanningDai/StrokeAvatar.git>. The repository contains all code necessary to reproduce the main experiments reported in this study.

Acknowledgements

S.G. acknowledges funding from the National Natural Science Foundation of China (grant No. 62171014), and Beihang University (grants No.KG161250 and ZG16S2103), which supported and hosted the core research activities reported in this work. L.G.O. acknowledges funding from EPSRC (grants No. EP/W024284/1, EP/P027628/1, EP/K03099X/1).

Author Contributions

Y.D. and S.G. conceived the idea and proposed the research. Y.D. and R.Z. developed and validated the algorithms. Y.Z., Y.W., and W.Y. performed the virtual simulations and visualizations. R.Z., W.Y., Jun.C., and X.C. tested, operated, and calibrated the motion-capture hardware system. R.X., Y.C., Q.L., Jin.C, T.L., and Y.P. recruited the participants and collected the locomotion database for modelling. C.T. and S.G. directed all the research. H.Z., X.G., A.N., P.S., and S.G. revised the manuscript. All authors wrote the manuscript, discussed the results and implications, and commented on the manuscript at all stages.

Competing Interests

The authors declare no competing interests.

References

- [1] Feigin, V.L. *et al.* Global, regional, and national burden of stroke and its risk factors, 1990–2021: A systematic analysis for the global burden of disease study 2021. *The Lancet Neurology* **23**, 973–1003 (2024).
- [2] Bernhardt, J. *et al.* The international stroke recovery and rehabilitation alliance. *The Lancet Neurology* **22**, 295–296 (2023).
- [3] Stinear, C.M. *et al.* Advances and challenges in stroke rehabilitation. *The Lancet Neurology* **19**, 348–360 (2020).
- [4] Feigin, V.L. *et al.* World stroke organization: Global stroke fact sheet 2025. *International Journal of Stroke* **20**, 132–144 (2025).
- [5] Poomalai, G. *et al.* Functional ability and health problems of stroke survivors: An explorative study. *Cureus* **15**, e33375 (2023).
- [6] Ferri, C.P. *et al.* Prevalence of stroke and related burden among older people living in Latin America, India and China. *Journal of Neurology, Neurosurgery & Psychiatry* **82**, 1074-1082 (2011).
- [7] Kisoli, A. *et al.* Levels of functional disability in elderly people in Tanzania with dementia, stroke and Parkinson's disease. *Acta Neuropsychiatrica* **27**, 206-212 (2015).
- [8] Feigin, V.L. *et al.* Pragmatic solutions to reduce the global burden of stroke: A world stroke organization–lancet neurology commission. *The Lancet Neurology* **22**, 1160–1206 (2023).

[9] Du, M. *et al.* Effectiveness of different exercise interventions on balance and cognitive functions in stroke patients: A network meta-analysis. *BMC Sports Science, Medicine and Rehabilitation* **17**, 250 (2025).

[10] Hatem, S.M. *et al.* Rehabilitation of motor function after stroke: A multiple systematic review focused on techniques to stimulate upper extremity recovery. *Frontiers in Human Neuroscience* **10**, 442 (2016).

[11] Langhorne, P., Bernhardt, J., and Kwakkel, G. Stroke rehabilitation. *The Lancet* **377**, 1693–1702 (2011).

[12] Donnellan-Fernandez, K., Ioakim, A., and Hordacre, B. Revisiting dose and intensity of training: Opportunities to enhance recovery following stroke. *Journal of Stroke and Cerebrovascular Diseases* **31**, 106789 (2022).

[13] Shimotori, D. *et al.* Influence of treadmill speed selection on gait parameters compared to overground walking in subacute rehabilitation patients. *Journal of Physical Therapy Science* **37**, 89–94 (2025).

[14] Gao, S. *et al.* Gait detection technologies. in *Wearable Systems-Based Gait Monitoring and analysis*, 27-100 (Springer, 2022).

[15] Tang, C. *et al.* An AI-Driven Multimodal Smart Home Platform for Continuous Monitoring and Assistance in Post-Stroke Motor Impairment. *IEEE Transactions on Neural Systems and Rehabilitation Engineering*. doi: 10.1109/TNSRE.2025.3645093 (2025).

[16] Islam, M.S. *et al.* Using AI to measure Parkinson's disease severity at home. *npj Digital Medicine* **6**, 156 (2023).

[17] Yu, B. *et al.* Quantifying impairment and disease severity using AI models trained on healthy subjects. *npj Digital Medicine* **7**, 180 (2024).

[18] Gonçalves, H.R. *et al.* Digital biomarkers of mobility and quality of life in Parkinson's disease based on a wearable motion analysis LAB. *Computer Methods and Programs in Biomedicine* **244**, 107967 (2024).

[19] Lange, F. *et al.* Computer vision uncovers three fundamental dimensions of levodopa-responsive motor improvement in Parkinson's disease. *npj Parkinson's Disease* **11**, 140 (2025).

[20] Salomon, A. *et al.* A machine learning contest enhances automated freezing of gait detection and reveals time-of-day effects. *Nature Communications* **15**, 4853 (2024).

[21] Zhang, W. *et al.* Wearable sensor-based quantitative gait analysis in Parkinson's disease patients with different motor subtypes. *npj Digital Medicine* **7**, 169 (2024).

[22] Lee, J. T. *et al.* Evaluation of performance of generative large language models for stroke care. *npj Digital Medicine* **8**, 481 (2025).

[23] White, A. *et al.* Predicting recovery following stroke: Deep learning, multimodal data and feature selection using explainable AI. *NeuroImage: Clinical* **43**, 103638 (2024).

[24] Scattolini, M. *et al.* Inertial sensing for human motion analysis: Enabling sensor-to-body calibration through an anatomical and functional combined approach. *IEEE Transactions on Neural Systems and Rehabilitation Engineering* **33**, 1853–1862 (2025).

[25] Seth, A. *et al.* OpenSim: Simulating musculoskeletal dynamics and neuromuscular control to study human and animal movement. *PLoS computational biology* **14**, e1006223 (2018).

[26] Zuo, C. *et al.* Self model for embodied intelligence: Modeling full-body human musculoskeletal system and locomotion control with hierarchical low-dimensional representation. In *2024 IEEE International Conference on Robotics and Automation (ICRA)* 13062–13069 (2024).

[27] Kettletley, S.A. *et al.* Speed-dependent biomechanical changes vary across individual gait metrics post-stroke relative to neurotypical adults. *Journal of NeuroEngineering and Rehabilitation* **20**, 14 (2023).

[28] Hayashi, Y. *et al.* Quadriceps muscle activity during walking with a knee ankle foot orthosis is associated with improved gait ability in acute hemiplegic stroke patients with severe gait disturbance. *Frontiers in Neurology* **15**, 1387607 (2024).

[29] Schulman, J. *et al.* Proximal policy optimization algorithms. *arXiv preprint arXiv:1707.06347* (2017).

[30] Ho, J. and Ermon, S. Generative adversarial imitation learning. *Advances in Neural Information Processing Systems* **29**, 4572–4580 (2016).

[31] Peng, X.B. *et al.* DeepMimic: Example-guided deep reinforcement learning of physics-based character skills. *ACM Transactions On Graphics (TOG)*. **37**, 143 (2018).

[32] Yue, J. *et al.* Human motion prediction under unexpected perturbation. *Proceedings of the IEEE/CVF Conference on Computer Vision and Pattern Recognition (CVPR)* 1501–1511 (2024).

[33] Gladstone, D.J., Danells, C.J., and Black, S.E. The Fugl-Meyer assessment of motor recovery after stroke: A critical review of its measurement properties. *Neurorehabilitation and Neural Repair* **16**, 232–240 (2002).

[34] Lei, W. Bridging Neuroscience and Clinical Practice: Accelerating stroke recovery in a pontine infarction case through neuroplasticity-based rehabilitation. *Cureus* **16**, e72563 (2024).

[35] Shi, C. *et al.* Effectiveness of treadmill training intervention for the management of patients with stroke: A systematic review and meta-analysis. *International Journal of Nursing Practice* **31**, e70020 (2025).

[36] Devittori, G. *et al.* Unsupervised robot-assisted rehabilitation after stroke: Feasibility, effect on therapy dose, and user experience. *Journal of Neuroengineering and Rehabilitation* **21**, 52 (2024).

[37] Tang, C. *et al.* A roadmap for the development of human body digital twins. *Nature Reviews Electrical Engineering* **1**, 199–207 (2024).

- [38] Choo, C.Z.Y., Chow, J.Y., and Komar, J. Validation of the Perception Neuron system for full-body motion capture. *PloS One* **17**, e0262730 (2022).
- [39] Carnegie Mellon University. CMU Graphics Lab Motion Capture Database. <https://mocap.cs.cmu.edu/> (2000).
- [40] Radosavovic, I. *et al.* Real-world humanoid locomotion with reinforcement learning. *Science Robotics* **9**, eadi9579 (2024).
- [41] Holden, D., Komura, T., and Saito, J. Phase-functioned neural networks for character control. *ACM Transactions on Graphics (TOG)* **36**, 1–13 (2017).
- [42] Wang, Y. *et al.* Skillmimic: Learning basketball interaction skills from demonstrations. *Proceedings of the IEEE/CVF Conference on Computer Vision and Pattern Recognition (CVPR)* 17540–17549 (2025).
- [43] Osa, T. *et al.* An algorithmic perspective on imitation learning. *Foundations and Trends® in Robotics* **7**, 1–179 (2018).
- [44] Bengio, Y. *et al.* Curriculum learning. *Proceedings of the 26th Annual International Conference on Machine Learning (ICML)* 41–48 (2009).
- [45] Peng, X.B. *et al.* ASE: Large-scale reusable adversarial skill embeddings for physically simulated characters. *ACM Transactions On Graphics (TOG)* **41**, 1–17 (2022).
- [46] Peng, X.B. *et al.* AMP: Adversarial motion priors for stylized physics-based character control. *ACM Transactions on Graphics (ToG)* **40**, 1–20 (2021).

Figures

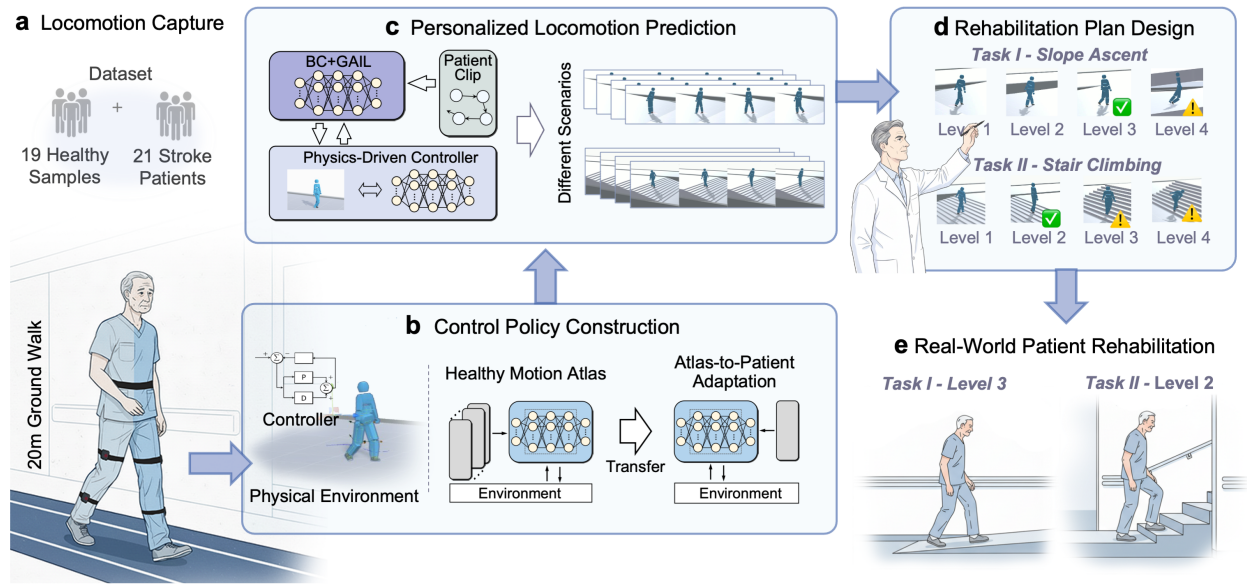


Figure 1 | Data-physics hybrid generative framework bridging simulation and real-world rehabilitation. Overview of the proposed generative framework, which constructs patient-specific control models from real-world walking data and generates physics-consistent locomotion predictions to inform rehabilitation decision-making. **a**, Baseline gait is recorded from a 20 m level-ground walk with wearable sensors, yielding joint kinematics, contacts, and interaction features for model initialization. **b**, An individualized control model is constructed by distilling the Healthy Motion Atlas as a population prior, followed by Atlas-to-Patient adaptation using a patient-specific walking clip. **c**, A data-physics hybrid generative model is built by coupling the personalized physics controller with behavioral imitation and GAIL-based adversarial learning, allowing patient-specific control patterns to predict locomotion across rehabilitation scenarios (e.g., slope, stairs). **d**, Clinicians review the predicted locomotion videos to assess task performances, determine safety margins, and select appropriate rehabilitation tasks and difficulty levels. **e**, Patients perform the selected training, and the personalized controller can be periodically refreshed with new walking assessments, enabling its use across multiple stages of rehabilitation.

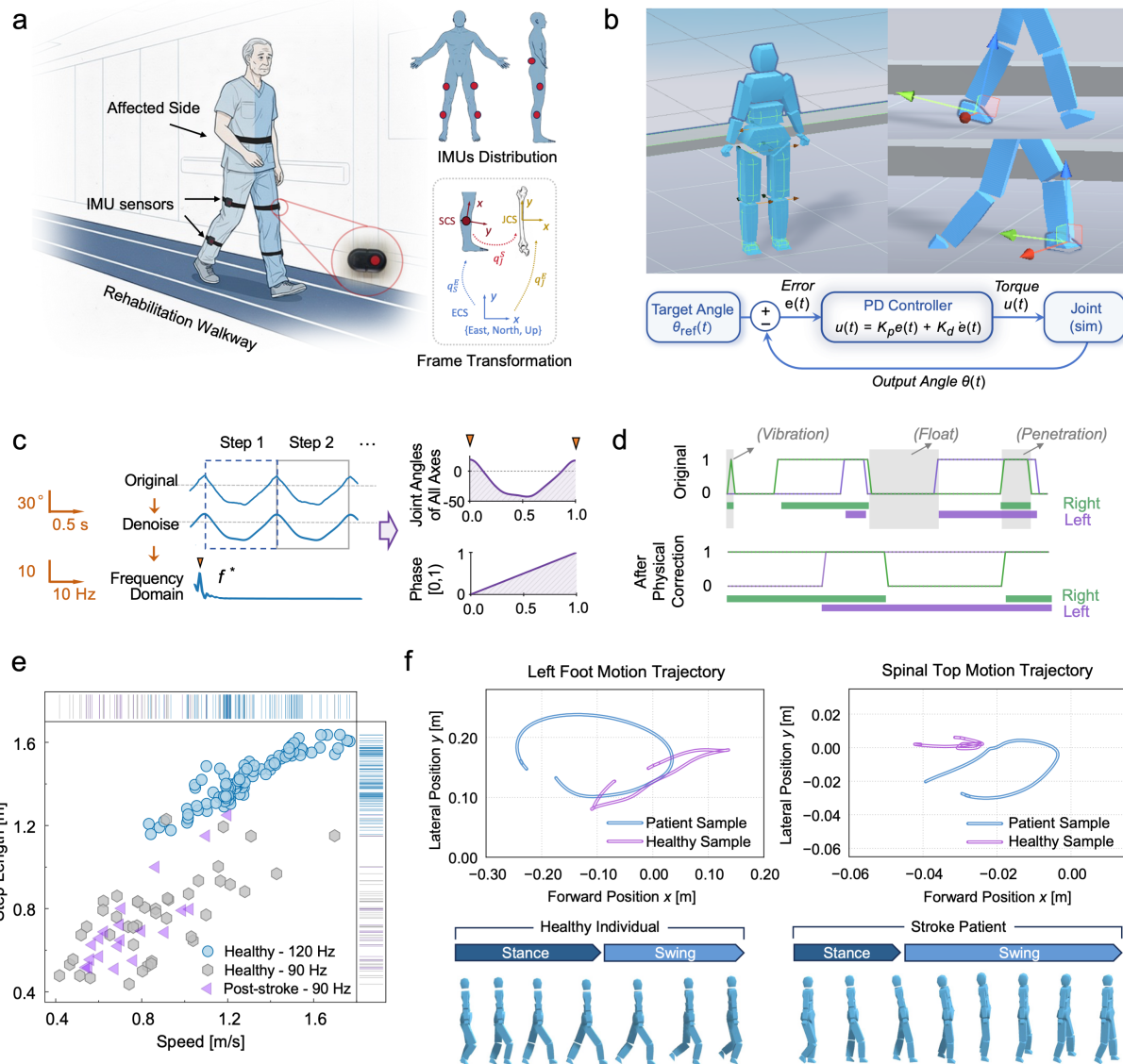


Figure 2 | Construction of the human locomotion dataset and physics-based control model. **a**, Experimental setup in which a patient walks along a rehabilitation walkway wearing IMU sensors on the pelvis, bilateral thighs, and bilateral shanks. A coordinated transformation chain between the Earth Coordinate System (ECS), Segment Coordinate System (SCS), and Joint Coordinate System (JCS) ensures anatomically consistent propagation of segment rotations and translations. **b**, Digital human avatar reconstructed from anatomical parameters, together with examples of IMU-induced artifacts such as floating and ground penetration, and a PD controller that generates joint torques from position and velocity errors. **c**, Gait-cycle segmentation performed via spectral-peak and extremum detection, illustrated with a representative segmented clip. **d**, Physics-based correction of foot-ground contact states to eliminate vibration, floating, and penetration artifacts. **e**, Step-length-speed distribution of the full locomotion dataset, combining captured data from healthy and post-stroke subjects as well as public gait databases. **f**, Comparison of healthy and patient trajectories in both foot and spinal-top motion, along with visualized walking sequences on the digital human model.

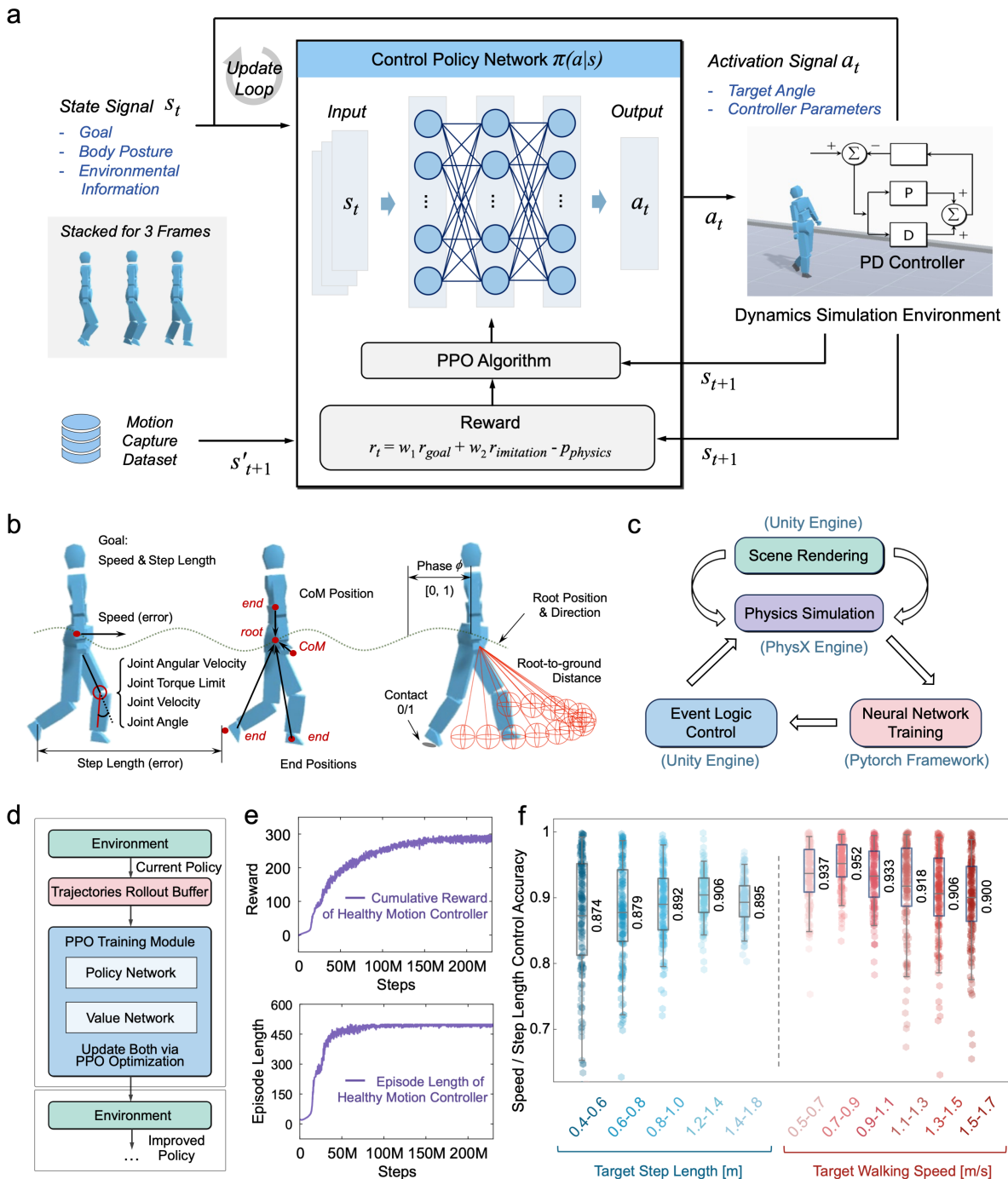


Figure 3 | Development of the Healthy Motion Atlas model via deep reinforcement learning.

a, Overview of the control-policy module, which receives sequential motion states and outputs proportional-derivative (PD) target signals for a 5-joint model. Training is performed in a closed-loop interaction with the physics environment, where the PPO algorithm updates the policy based on the state transitions and rewards. **b**, Composition of the state vector, including goal variables

(target speed and step length), global gait descriptors, segment kinematics (joint angles, angular velocities, torques), and environment cues such as foot–ground contact and root-to-ground distance. **c**, Integrated training pipeline coupling Unity-based scene rendering and PhysX simulation with PyTorch neural-network optimization, where event logic and policy updates are synchronized each frame. **d**, PPO training loop: the current controlling policy repeatedly interacts with the environment to collect trajectories, which are stored in a rollout buffer and then used by the PPO training module to update both the policy and value networks. **e**, Training curves showing progressive increases in cumulative reward and episode length as the controller converges. **f**, Accuracy distribution of the trained Healthy Motion Atlas model across different target step lengths and walking speeds.

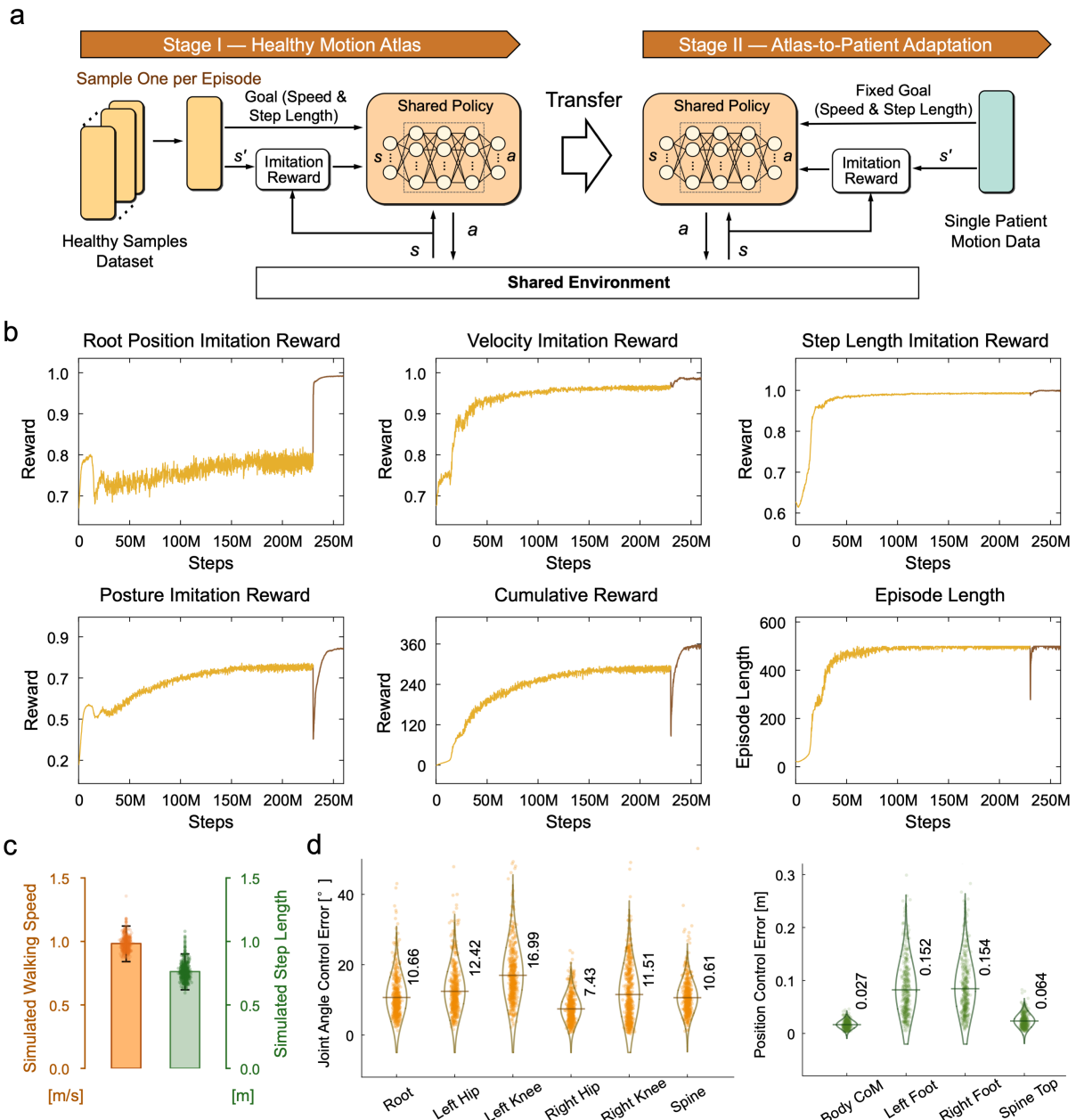


Figure 4 | Atlas-to-patient adaptation via goal-conditioned transfer learning. **a**, Adaptation scheme in which the Healthy Motion Atlas initializes the controller, and personalization is achieved by updating task goals (target speed and step length). **b**, Training curves showing rapid gains across all imitation objectives and cumulative reward, while episode length remains consistently high, indicating fast personalization and stable control performance enabled by the Healthy Motion Atlas. **c**, Comparison between the representative patient's measured gait parameters and the personalized controller's outputs, showing high-fidelity reproduction of walking speed (1.02 m/s vs. 0.98 m/s) and step length (0.80 m vs. 0.76 m). **d**, Distributions of joint-angle control error across all lower-body articulations, together with position-error distributions for the body center of mass and distal end points under the personalized controller summarized across the model-assisted group.

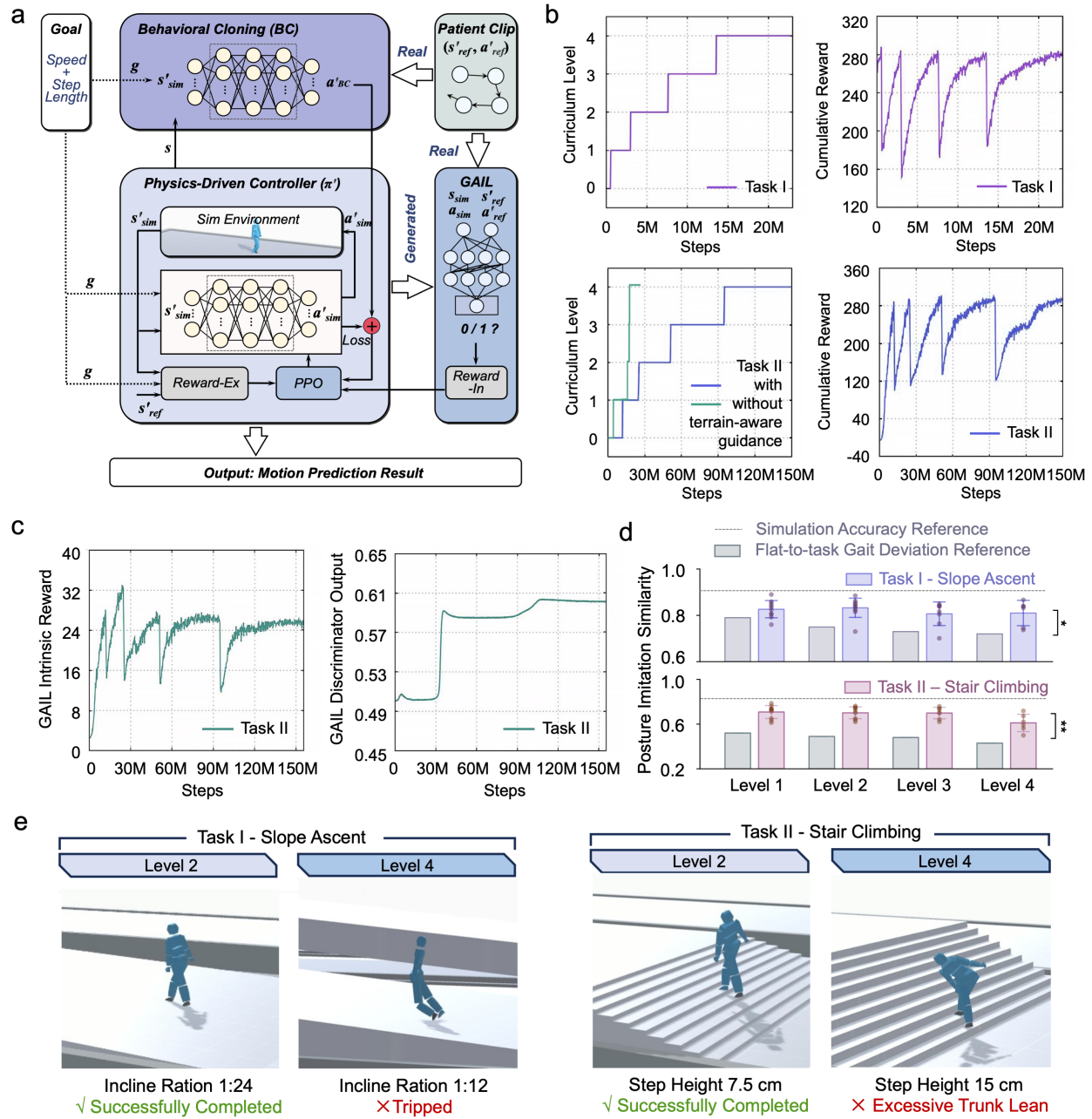


Figure 5 | Terrain-adaptive locomotion prediction and rehabilitation plan design. **a**, Data-physics hybrid generation framework that operates on patient-specific data, combining a personalized physics-driven controller with behavioral cloning and a GAIL network to maintain consistent activation patterns across motion; curriculum tasks are defined across difficulty levels spanning slopes and stairs. **b**, Curriculum progression and reward curves during training for slope and stair tasks, indicating the relative difficulty and learning time required at each level. **c**, GAIL intrinsic reward and discriminator output during stair-task adaptation, showing improved alignment between generated and real motion patterns, with imitation consistency reaching 79.7%. **d**, Posture prediction accuracy evaluation across 11 personalized models, comparing predicted motions with recorded patient trajectories under different tasks and difficulty levels. Significance is evaluated relative to the task-dependent lower-bound baseline, with $p < 0.05$ (*) and $p < 0.01$ (**) indicated.

(**). e, Visualized rollouts illustrating example outcomes across difficulty levels, showing stable execution at appropriate difficulty and the emergence of compensatory or unstable behaviors (such as tripping or excessive trunk lean), when the task becomes too demanding.

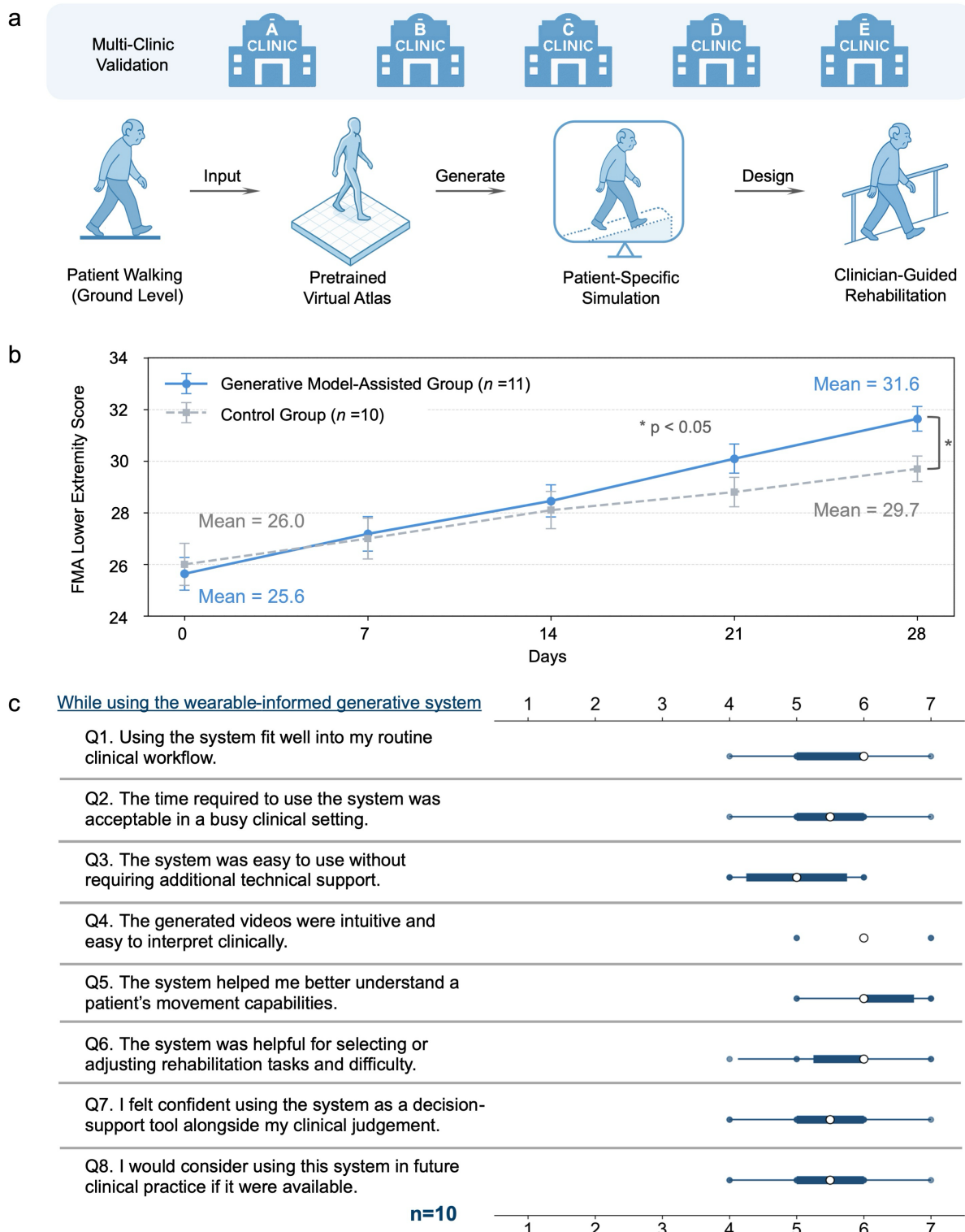


Figure 6 | Clinical integration and rehabilitation outcomes. a, Deployment of the data–physics hybrid generative model within a clinical rehabilitation workflow. Upon patient admission, gait data are collected during a 20 m walking test to construct an individualized model. The system

simulates rehabilitation tasks of varying difficulty to support clinician-in-the-loop treatment planning. **b**, Pilot randomized study in 21 inpatients with post-stroke lower-limb impairment (generative-model-assisted group, $n = 11$; control group, $n = 10$). All patients received standard lower-limb rehabilitation for 28 days; only therapists in the model-assisted arm had access to model predictions during planning. Fugl-Meyer Assessment lower-extremity (FMA-LE) scores (mean \pm s.e.m.) improved in both groups, with larger gains in the model-assisted group (baseline means: 25.6 vs 26.0; day-28 means: 31.6 vs 29.7; $*p < 0.05$ between groups at indicated time points), suggesting that generative-model-based decision support may enhance functional recovery. **c**, Therapist feedback collected after using the system to support rehabilitation planning, rated on a 7-point Likert scale (1 = strongly disagree; 7 = strongly agree) across eight items covering workflow integration, time burden, ease of use, interpretability of generated videos, perceived clinical usefulness, decision-support confidence, and adoption intention. Dots represent individual responses; thick bars denote the interquartile range (IQR), whiskers indicate $1.5 \times$ IQR, and white circles mark the median. Higher scores indicate greater usability and perceived clinical value. $n = 10$ therapists.